International Journal of Astrobiology 5 (1): 47–56 (2006) Printed in the United Kingdom
doi:10.1017/S1473550406002874

Spectral analyses of sabkha sediments with implications for remote sensing on Mars

F.M. Howari

Geology Department, Faculty of Science POB 17551, UAE University, Al Ain, United Arab Emirates
e-mail: fhowari@uaeu.ac.ae
Southwest-Applied Earth and Environmental Services, POB 155144, Irving, TX 75015, USA

Abstract: Spectroscopic investigations of surface mineral components, expected to exist on the surface of Mars, using multiple spectral ranges and techniques, are vital to obtain the ground truth information or reference data for Mars exploration missions. This paper presents visible, near-infrared, thermal infrared reflectance and thermal infrared transmission spectra, as well as X-ray diffraction and scanning electron microscope/energy dispersive X-ray analyses of salt crusts and sediments interleaved with cyanobacterial materials from a coastal zone of the United Arab Emirates, where sabkhas exist. The samples obtained from sabkhas were characterized because they contain minerals requiring the water for formation and they provide a possible environment for some of the earliest organisms on Earth. The surface minerals identified include gypsum, calcite, halite, aragonite and dolomite. These sediments were found to be mixed with each other and intermingled with an algal mat, which consisted of cyanobacteria. If such materials formed in similar environments on Mars, their identification would be important for understanding the geobiological conditions of the planet and the potential habitability for life.

Received 4 December 2005, accepted 4 May 2006

Key words: an algal mat, cyanobacteria, evaporite, Mars, reflectance spectroscopy, remote sensing, sabkhas, salt.

Introduction

In the field of remote and *in situ* mineral identification, visible and infrared spectroscopy are highly successful techniques for mineral identification of geologic materials on Earth and Mars (Crowley 1991; Clark 1999; Howari *et al.* 2003; Mahaney *et al.* 2004). Landed missions to Mars have employed spectroscopic and other mineral identification techniques in order to study the surface components and associated environmental conditions (e.g. Christensen *et al.* 2004a,b; Squyres *et al.* 2004a,b; Arvidson *et al.* 2005; Bibring *et al.* 2005; Gendrin *et al.* 2005; Mustard *et al.* 2005). For example, the infrared spectral analyses from the Viking and Pathfinder missions indicate possible occurrences of salts on the Martian surface in soils, cements, rocks and dust in the atmosphere, which has significant proportions of Na and Cl (Lane & Christensen 1998; Gilmore *et al.* 2004; Bishop *et al.* 2004; King *et al.* 2005). Other research on Martian brines proposes that there may be several sites on Mars where hypersaline waters may exist in the shallow crust, thus creating the potential near the surface for an environment for life (Pierson & Parenteau 2000; Ruff *et al.* 2001; Bishop *et al.* 2004; Edwards *et al.* 2005a,b; Villar & Edwards 2005). Remote characterization and the location of these spots have important future applications regarding site selection of astrobiological missions to Mars (e.g. Bell 1996; Russell *et al.* 1998).

On Earth, the occurrences of the sabkha environment (salt-flat areas) and their deposits indicate the presence of extreme environments of high salinity and surface temperature where water and intensive evaporative processes affect the shallow subsurface (e.g. Evans *et al.* 1969; Friedman & Krumbein 1985; Alsharhan & Kendall 2002). Various sediment facies are formed in this environment by certain physicochemical processes. The main litho-type produced in these environments are the evaporites, consisting of several salts with high albedo such as halite and gypsum (Evans *et al.* 1969; Alsharhan & Kendall 2002; Howari *et al.* 2003). High-albedo areas have been recognized on the Martian surface owing to superficial deposits; others have been identified in layered deposits within basins (Christensen 2003; King *et al.* 2005). These high-albedo zones could be the remnant of sabkha or dusty materials composed of iron oxides, sulphates and other evaporates. However, evaporitic sediments usually display a very high albedo owing to lack of absorption along various portions of the electromagnetic spectrum, especially in the $\sim$400 and 1000 cm^{-1} spectral region (Lane & Christensen 1998; Crowley 1991; Roush *et al.* 1993; Drake 1995). These sediments usually have high concentrations of Na^{+}, Mg^{+2}, Ca^{+2}, Cl^{-} and/or SO_4^{-2} solutions. The physics of the atomic and molecular vibration processes are important in creating the absorption features necessary for their identification (Hunt 1982; Howari 2004).

According to Landis (2001), any liquid water on Mars would have to be a highly concentrated brine solution. It is probable, therefore, that any present-day Martian microorganisms would be similar to terrestrial halophiles or extremophiles. The sediment samples studied have a distinctive spectral signature owing to the vibration absorption features and photosynthetic pigments of the stratified microbial community that populate the sabkha environment. With this in mind, it becomes a reasonable speculation to expect that Mars' surface would have similar composition. However, it would be an interesting exercise to use hyperspectral imaging to look on Mars for the spectral signature of halobacteria mingled or associated with evaporites. An observation which is more likely to produce useful results would be to search for the spectral signature of salts, in order to identify salt-flat locations (playa) where salt and halobacteria would be located (e.g. Landis 2001). If the presence of halophiles or extremophiles was proven to be true without speculation, it would then become justifiable to address the additional issue of whether this pronounces the beginning of life on Mars, or whether life has already begun and these organisms are derived from ancestors that could not tolerate such environments.

The present study used several spectroscopic and microscopic techniques such as X-ray diffraction (XRD), visible near-infrared (VNIR), thermal infrared (TIR), Fourier transform infrared (FTIR) and scanning electron microscopy (SEM) images in order to characterize these sabkha sediments. Spectral analyses of samples from sabkhas of the United Arab Emirates (UAE) provide remote-sensing information useful in searching for sabkhas environments on Mars using current and upcoming datasets. However, understanding the spectral mode of formation of the investigated samples may be critical for interpreting the spectral characteristics of Mars objects in a wide electromagnetic or spectral range. The presented data will also help to identify the type of spectral measurements and instrumentation that will be needed to detect such environments on Mars during future missions, and will assist in interpreting some of the data from Mars (e.g. Lane & Christensen 1998; Bishop *et al*. 2004). In essence, the sediments of the sabkha regions studied here may provide a new analogue for potential habitable sites on Mars. The study demonstrates the potential of specific tests that could be made in the Martian environment to test for life forms or fossils from a rover or from orbit – in those areas where there are bright, bedded, evaporite-rich deposits (e.g. sulphates). However, connecting this work in detail to the current results from Mars returned from the Mars Exploration Rover and Mars Express is beyond the scope of this short paper.

Location of the study area

The study area is located between 20° 50′ and 26° N and 51° and 56° E, with an average slope of 1:3000. It is situated along the coastal area of Abu Dhabi Emirate, extending to the west-southwest region of Abu Dhabi City, UAE. The terrestrial area is characterized by the presence of flat, salt-encrusted surfaces covered by a thin layer of blue-green algae, and abundant mangrove trees. The monthly average air temperature of the coasts in the vicinity of Abu Dhabi averages from 47 °C in summer to 12 °C in winter. Although abundant, the mangroves grow in this area with variable density. Figure 1 shows the location of the studied sabkhas together with a Landsat ETM+ image; the white spots in this image represent salt crusts and other evaporites.

Methods

The VNIR, spectra were run on a Perkin Elmer 900 spectrometer[1] collecting hemispherical reflectance measurements from 0.4 to 2.5 μm (25 000–4000 cm^{-1}). 'Spectrolon'[1] (similar to MgO) was used as the 'white reference' background. The emittance TIR spectra were run on a Thermo-Nicolet Nexus 670 FTIR spectrometer[1], with a gold integrating sphere, collecting hemispherical reflectance measurements from 2.5 to 15 μm (666–4000 cm^{-1}). Liquid nitrogen was used as the detector coolant and aluminium foil as the reference background. All samples were run at USGS Laboratories at Reston, VA, USA as bulk separates using a sample holder of a few centimetres in diameter. The results were compared with published spectral libraries and profiles (http://speclab.cr.usgs.gov; http://speclib.jpl.nasa.gov; Crowley 1991; Gaffey *et al*. 1993; Lane & Christensen 1998; Clark 1999; Howari *et al*. 2003). The reference and target samples were placed so as to completely fill the field of view of the instrument. The peaks were determined using the Clark and Roush (1984) method. The transmittance FTIR spectra of selected dissolved samples were obtained by a Nicolet FTIR 560[1] system housed at the Central Laboratory of UAE University. XRD techniques were used for the identification of the mineral components of the silt size fraction of the studied sabkhas. The evaporite samples were examined in the range of 2θ of 2–60° under the following conditions: Cu tube operated at Kv = 40, Am = 40, diffractometer operated at a scanning rate of 1° min^{-1} and the chart recorder at a rate of 1° cm^{-1}. The evaporite minerals were identified according to their basic reflections as given in the American Society for Testing and Materials cards index. The collected samples were examined under the binocular microscope. Before examining the samples by SEM for crystal morphology and nanoscale features, the samples were mounted to a stup using double-sided sticky tape and then gold coated using a sputter coater. Energy dispersive X-ray (EDX) analysis was also performed on the samples inspected by the SEM.

[1] Perkin Elmer 900 spectrometer (PerkinElmer Life And Analytical Sciences, Inc., USA); Spectrolon (Spectrolon-Labsphere Inc., North Sutton, NH, USA); Thermo-Nicolet Nexus 670 FTIR spectrometer, (Thermo Electron Corporation); Nicolet FTIR 560 (Thermo Electron Corporation).

https://doi.org/10.1017/S1473550406002874 Published online by Cambridge University Press

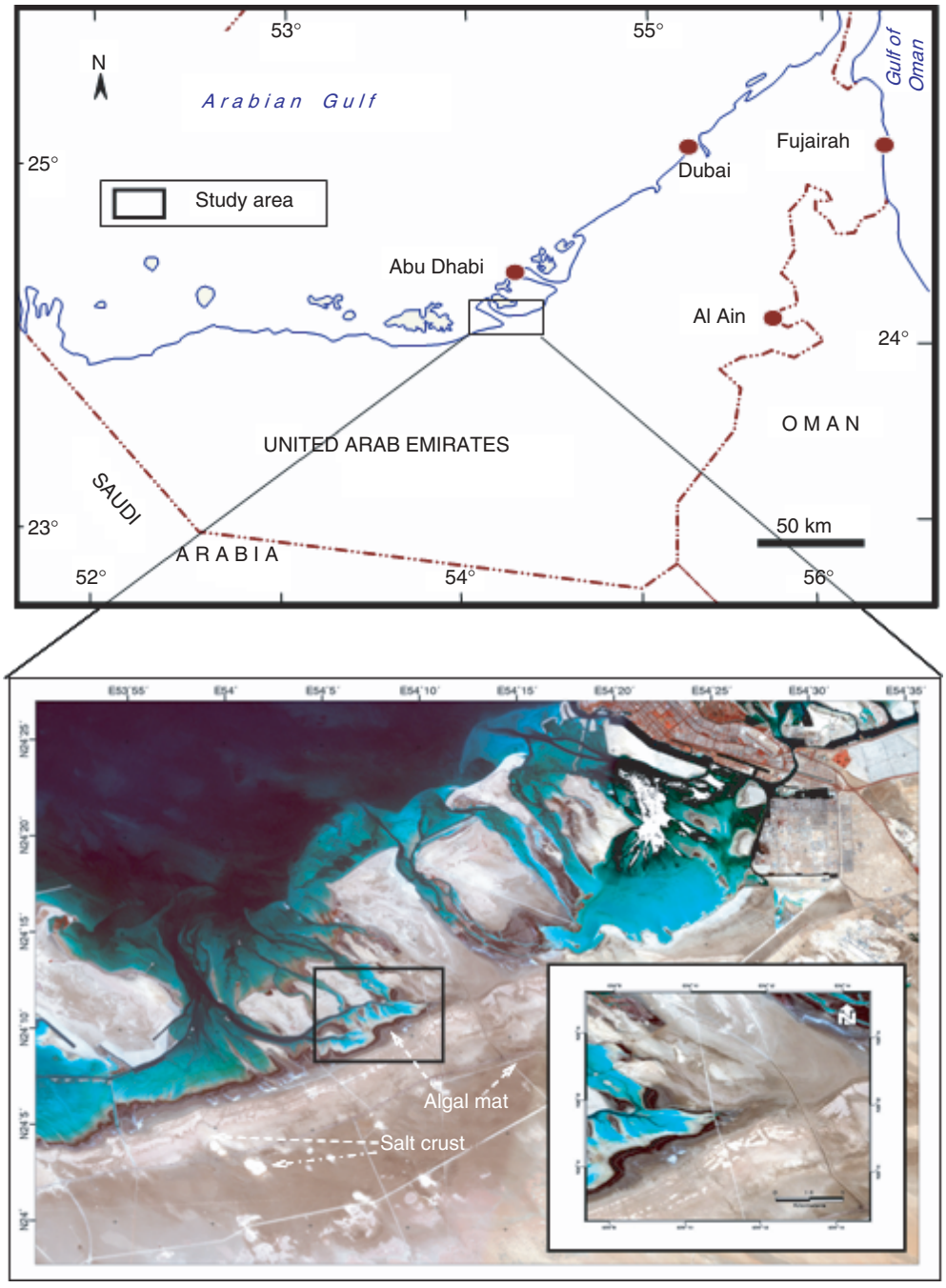

Fig. 1. Location map of the study area with RGB landsat ETM+ image.

Results and discussion

Macromorphology

Figure 2, shows different views of the studied sabkhas. The sabkhas are covered by a salt crust, 3–5 cm thick, under which there lies 25–150 cm of carbonate sand, gypsum and halite. Some of the salt crust has an irregular, knobbly surface with irregular polygonal patterns (Fig. 2). The edges between adjacent polygons turn upwards abruptly (Figs 2(a)–(d)). Gypsum crystals embedded within halite crystals were observed in the study area (Figs 2(e) and (f)). Sandy texture sediments with laminated algal mats covered with a salt crust about 150 cm thick and the occurrences of gas bubbles were also observed (Fig. 2(h)). The gas domes are the surface expression of sediment compaction because of rapid deposition of sand-size materials containing large amounts of trapped water and air. During compaction, the water and air are expelled from the sediment together with any gas generated by decaying organic matter. However, different types of algal mats were observed at the surface of the investigated sabkhas as flat mats (Figs 2(g) and 3). They are visible as a lower wet sub-zone and an upper dry

https://doi.org/10.1017/S1473550406002874 Published online by Cambridge University Press

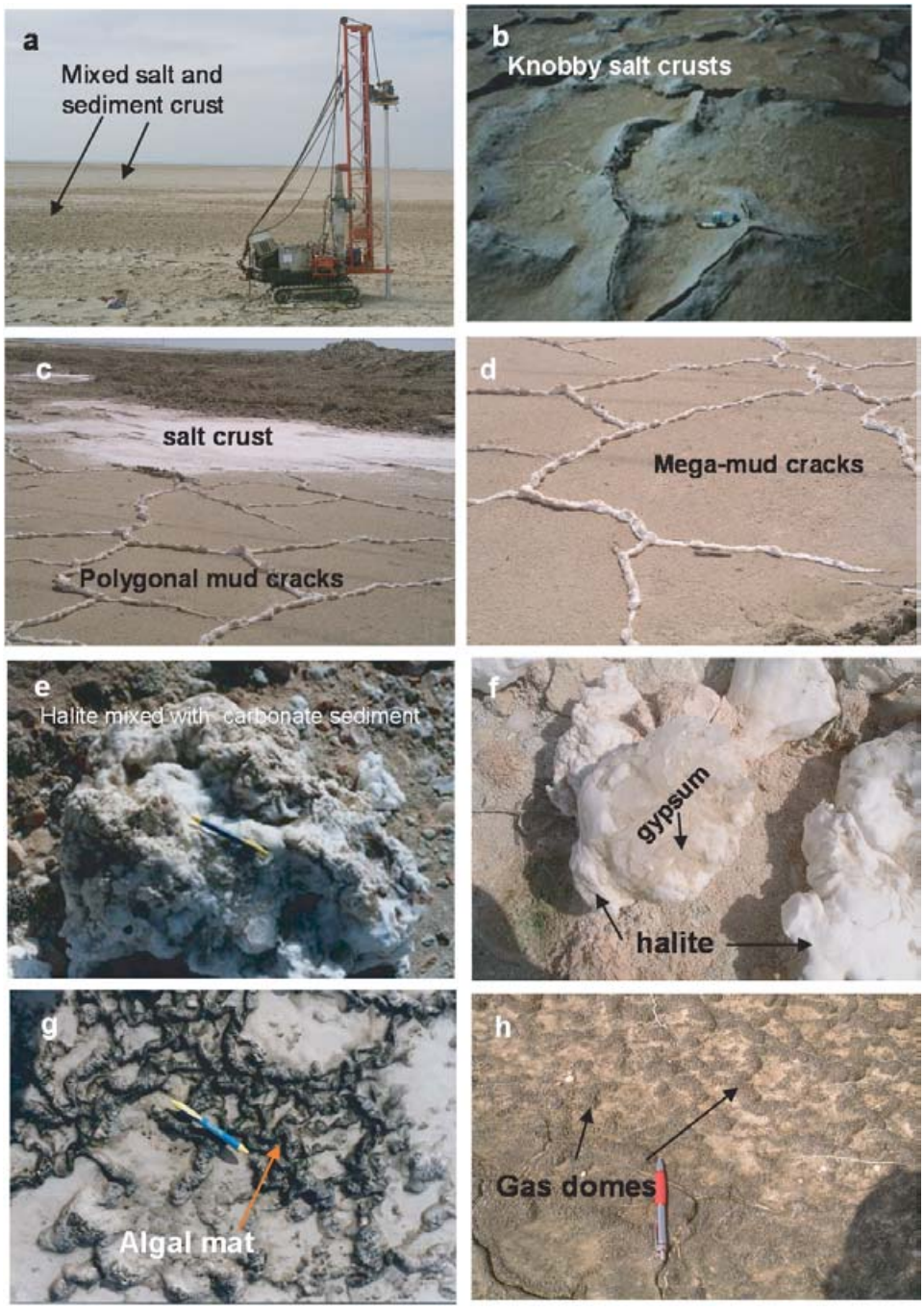

Fig. 2. Different views of the investigated sabkhas, and location of selected samples.

sub-zone. The wet one has a green colour, whereas the dry one has a black to dark-brown colour and is covered by halite (Fig. 3).

Micromophology

The micrographs presented in Fig. 3 show several layers in the an algal mat samples; the inner layer is formed from folded algal mats, whereas the outer layer is formed from salts. The algal mats are composed of cyanobacterial microfilament accumulations in the form of mats, which have an average width of approximately 2 km and can reach a thickness of at least 30 cm (e.g. Alsharhan & Kendall 2002). As observed from the X-ray analyses, some sites have slight variations from this composition; they have various contents of carbonate sand with halite, gypsum and dolomite (Fig. 4). The crystal morphology and nanoscale features of the samples studied are shown in Fig. 5. The SEM reveals a generalized development of layers of cyanobacteria that contain authigenic and detrital minerals. The fibrous texture

https://doi.org/10.1017/S1473550406002874 Published online by Cambridge University Press

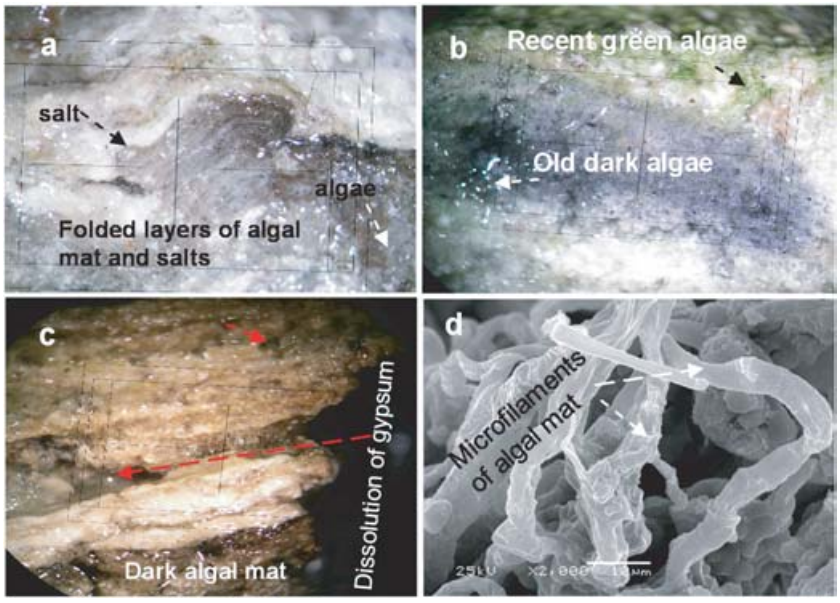

Fig. 3. Cross sections of the algal mat present in the study area.

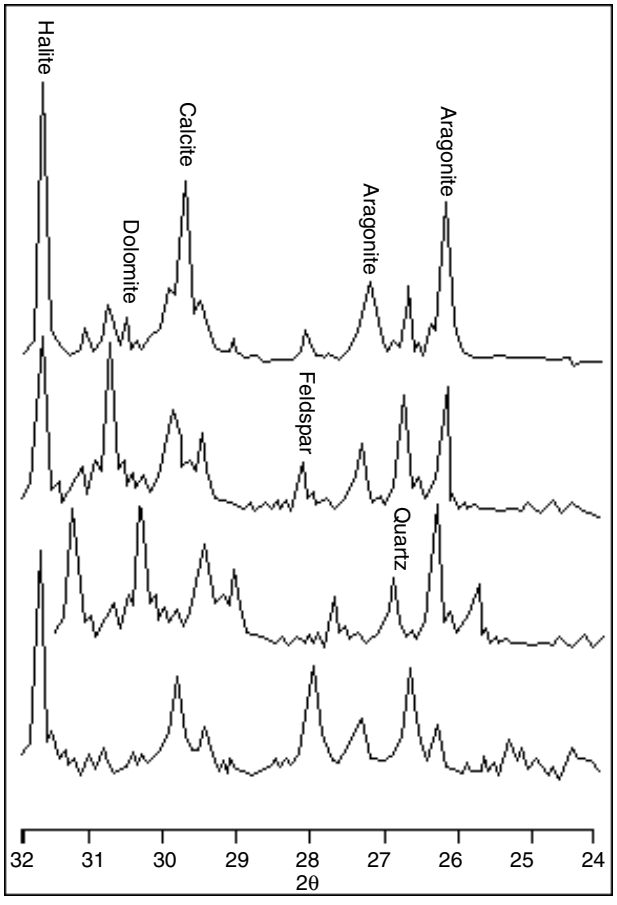

Fig. 4. X-ray profiles of the collected samples from the studied sabkhas.

of some of the calcium-rich grains suggests the presence of authigenic aragonite. Most of the samples contain microfilaments intermingled with halite and carbonates in different proportions. Calcite crystals encrusted with silicate coating are observed from the SEM images and associated EDX analyses (Fig. 5(c)). EDX analyses demonstrate the presence of Mg, and Si corresponds to traces of dolomite and silicate minerals. Halite and calcite grains coated with microbial mat and branching filaments of well-developed cyanobacterial mat accumulations were also observed in the study area. Secondary growths of what was probably calcite cement were found within the vents of the algal structure and around halite crystals (Fig. 2(e)).

VNIR-SWIR spectra

Spectroscopic measurements in the VNIR-SWIR region have been used for mineral identification in a number of studies of pure minerals (Gaffey *et al.* 1993; Hapke 1993; Clark 1999; Howari 2004) and natural samples containing multiple minerals and/or species (Hunt 1982; Crowley 1991; Howari *et al.* 2003; Bishop *et al.* 2004). This spectral region is particularly well suited for identification of coloured minerals. Iron and other transition metals in minerals exhibit spectral features due to electronic transitions that produce characteristic bands (Clark 1999). The OH, carbonate and sulphate groups in minerals produce characteristic spectral features in this region owing to overtones and combinations of the molecular vibrations (Gaffey *et al.* 1993; Clark 1999; Howari *et al.* 2003; Bishop *et al.* 2004).

The VNIR reflectance spectra of the collected samples shown in Fig. 6 were comparable in terms of the position of the absorption features with those published in the literature (Drake 1995; Metternicht & Zink 1997; Clark 1999; Howari *et al.* 2003). The spectra of the samples are dominated by gypsum spectral bands, and the spectra of other samples contain features characteristic of gypsum as well as organic stretching bands. Samples 6L and 8L represent spectra of evaporates (contaminated halite with gypsum) mixed

https://doi.org/10.1017/S1473550406002874 Published online by Cambridge University Press

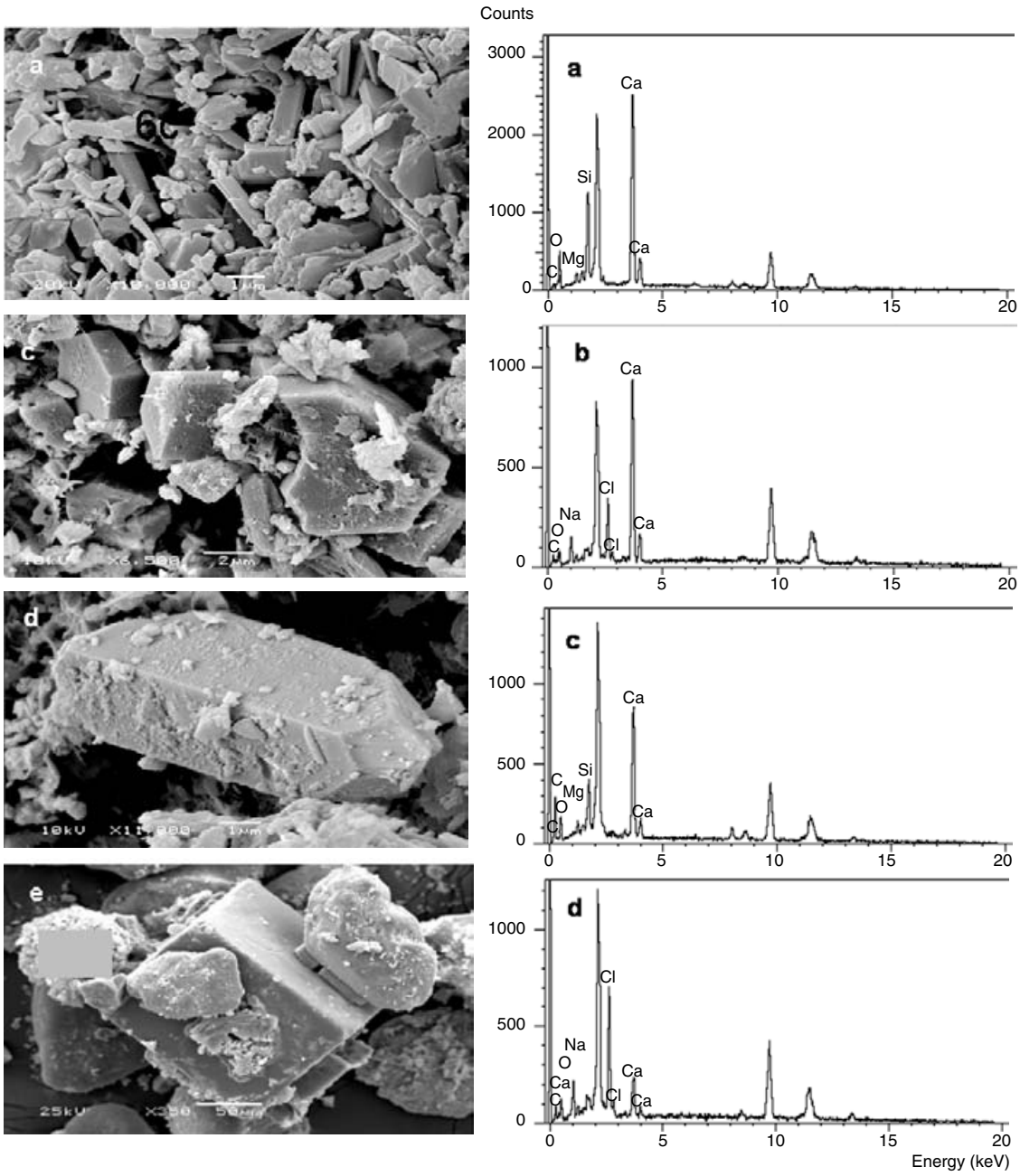

Fig. 5. SEM photomicrograph of sabkhas samples and associated EDX results.

with an algal mat and traces of dolomite at different proportions.

Sample number 10L (Fig. 6) represents a textbook example of gypsum spectra. In this sample the overtones or combination tones from fundamental vibrations of the water molecules produced a series of bands affecting the infrared spectrum between 1 and 2.3 μm (e.g. 1.464, 1.550, 1.750, 1.978 and 2.300 μm), and these can be detected in the spectra of gypsum crusts (Fig. 6). These are the locations within the VNIR-SWIR spectra that are best for detecting gypsum. However, the most dominant absorption features occurred at 1.464, 1.750 and 1.978 μm; in addition, two small peaks maintain a consistency in appearance at 1.755 and 1.865 μm. These findings are in agreement with earlier findings of Hunt *et al*. (1971a); Hunt (1982); Mulders (1987); Mougenot *et al*. (1993) and Clark (1999). It was observed that, by increasing the portion of halite (40%) and an algal mat (30%), the absorption feature between 1 and 1.5 μm disappeared (e.g. sample number 7L). Samples numbered 2L to 5L as well as 9L represent spectra of gypsum (60%) mixed with an algal mat (30%). Halite itself (e.g. sample number 7L) cannot induce absorption bands in the visible and near-thermal infrared (Hunt *et al*. 1971a,b; Mougenot *et al*. 1993). Water bands (1400, 1900 and 2250 nm) were observed in the spectra

https://doi.org/10.1017/S1473550406002874 Published online by Cambridge University Press

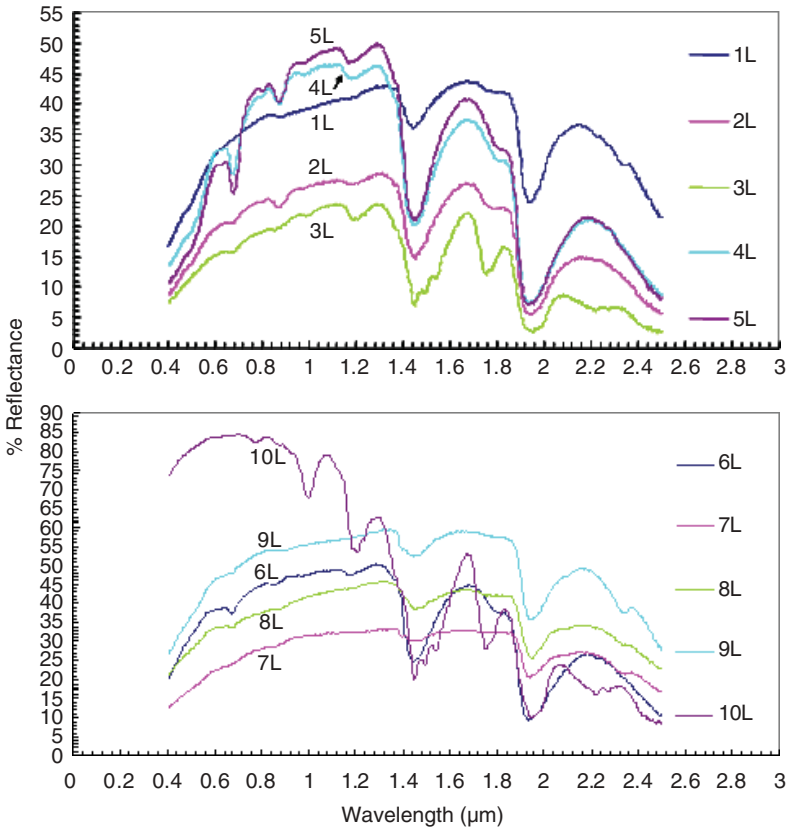

Fig. 6. VNIR reflectance spectra of samples from the investigated sabkhas.

of halite crusts (Fig. 6) owing to moisture and fluid inclusions, and these are the dominant absorption features of halite. Similar results were found in Hunt *et al.* (1971a); Mulders (1987) and Mougenot *et al.* (1993).

Emittance spectra

The emittance TIR spectra of the samples are given in Fig. 7. The main spectral absorption features in the TIR range arise from the S—O bond oscillations of the sulphate anion. The diagnostic sulphate features occur at 490, 680, 600 and 1160 cm^{-1}. Halite is an isometric crystal with three equal-length axes that are orthogonal to each other. Thus, the energy emitted from any direction is identical. The entire crystal lattice of halite vibrates as a whole. The typical spectrum of halite has a broad absorption band at frequencies higher than 600 cm^{-1} (>15 μm) (Lane & Christensen 1998). For example, sample number 10L, which represents gypsum, has absorption features at 3.9, 4.8, 5.9 and 9 μm, and very weak features at 15 and 17 μm. The algal-mat-dominated spectra have diagnostic absorption features between 3.3 and 5 μm (2000 and 3000 cm^{-1}) (e.g. 1L, 4L and 7L). The TIR spectra are complicated by a combination of what are apparently grain-size effects. The spectra from 10L, 2L and 5L appear similar to large crystal faces, while those from 1L, 7L, 8L and 9L are more consistent with fine grain sizes. In these samples the deep absorption feature near 3.4 (2941 cm^{-1}) is related to the C—H stretch. Samples 5L, 2L and 4L, as well as 10L, do not show active absorption features between 1300 and 3500 cm^{-1}. However, we expected to observe obvious features in the TIR range that arise from the C—O bonds as the XRD and SEM indicate, but these were not detected. This could be due to the fact that remote-sensing spectroradiometric techniques average the spectral features of the targets in the field of view, whereas XRD and SEM use very low numbers of beams. Thus, it is difficult to directly relate the spectra between different measurement techniques unless the sample materials are identical.

Dissolved FTIR spectra

The transmittance FTIR spectra of selected samples are given in Fig. 8. The identification of absorption bands was carried out based on data published by Stevenson (1994), Barancikova *et al.* (1997), Haskin *et al.* (1997), Russell *et al.* (1998), Sobalik *et al.* (1998), Hunt & Salisbury (1970), Howari *et al.* (2003), Klingelhöfer *et al.* (2003), Howari (2004) and Pérez *et al.* (2004). The most important features are the broad band at 3429 cm^{-1} associated with the O—H stretch of OH groups, the peak at 2924 cm^{-1} due to aliphatic C—H stretching, the weak feature at 1716 cm^{-1} attributed to C═O stretching of COOH and ketones, and the strong peaks at 1622 cm^{-1} associated with structural vibrations of aromatic C═C and the antisymmetrical stretching of COO— groups and at 1115 cm^{-1} associated with C—O stretching and O—H bending of COOH groups. The peaks occurring

https://doi.org/10.1017/S1473550406002874 Published online by Cambridge University Press

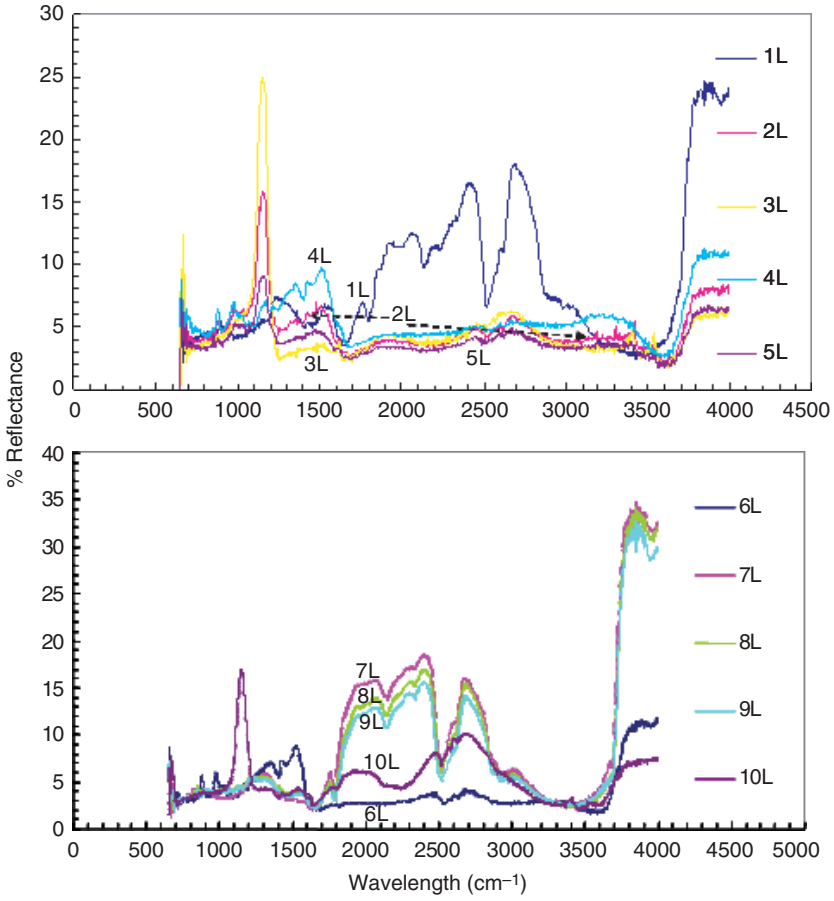

Fig. 7. TIR reflectance spectra of samples from the investigated sabkhas.

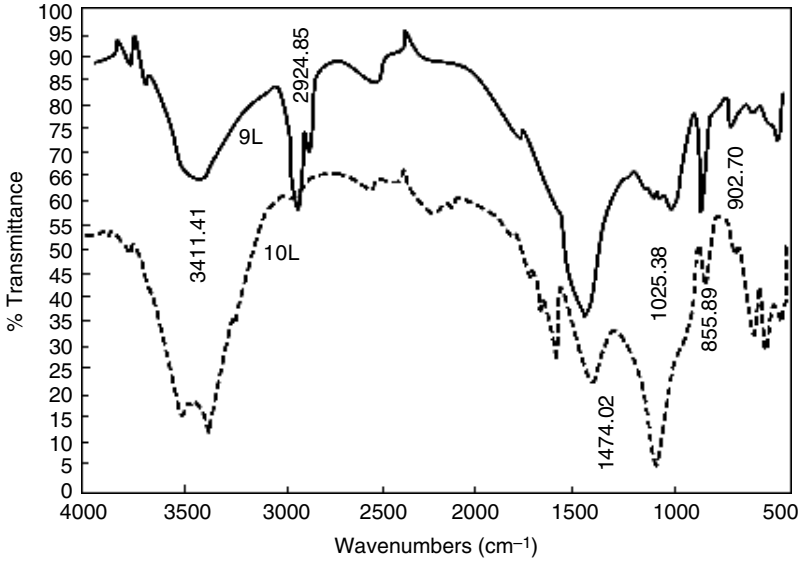

Fig. 8. FTIR transmittance spectra of samples from the investigated sabkhas.

occasionally at 959 and 1000 cm^{-1} are attributed to Si—O vibrations of silicate impurities (Stevenson 1994; Pérez *et al.* 2004).

Overall, the sabkha samples contain overtones of stretching vibrations near 1.46 μm, besides the water stretching and bending combination band near 1.95 μm. Additional features are attributed to aliphatic C—H stretching vibrations and these are consistent with the presence of organics from the EDX and microscopic analyses. A sharp absorption band near 0.67 μm in the spectra of some samples such as 4L, 5L,

https://doi.org/10.1017/S1473550406002874 Published online by Cambridge University Press

6L and 8L could be related to chlorophyll, a pigment of the an algal mat (Bishop *et al*. 2004). The hydrocarbons and chlorophyll bands are attributed to organisms living in the sabkhas. The total organic carbon (TOC) analyses in the study area indicate that the TOC of the samples shows a wide range of organic enrichment (0.95–12.070 % TOC) indicating an excellent quantity of organic matter productivity (Sadooni *et al*. 2005).

The suites of samples reported in this study most closely represent the chemistry of the salts predicted for Mars on the basis of previous published data (Clark & Van Hart 1981; Dreibus & Wnke 1990; Clark 1993; McSween *et al*. 1999; McLennan 2000; McSween & Keil 2000; McSween 2002; McLennan 2003; McSween *et al*. 2003). Many of the minerals present in sabkahs, such as gypsum and dolomite samples, may be associated with organisms and/or provide information about environments supportive of life on Mars. Identification of salt-flat areas on Mars would be important for understanding the geology of the planet and potential habitability for extinct or extant life. Moreover, integrating multiple spectroscopic techniques provides comprehensive mineralogy information owing to the maximum coverage of excitational and vibrational bands at all wavelengths (e.g. Haskin *et al*. 1997). The current orbital and landed missions to mars are enabling correlation of both the VNIR and mid-IR regions, making the creation of combined spectral datasets of Mars analogues more important. The types of measurement presented and the sample material are of interest to the astrobiology community for ground truth information or reference data and interpretation of terrestrial data sets, and as a possible analogue to Mars.

Conclusion

The reported data and related literature review indicate that the mineral phases present in sabkha samples are associated with organisms and thus might be of benefit as indicators of past life or environments supportive of life on Mars. The spectral analyses (e.g. the documented wavelength regions, associate absorption features and interpretations) from sabkhas can provide a resource of potential geo-biosignatures for remote spectroscopic analyses of particular interest for future exploration missions of Mars. The reported spectral signatures are mostly due to water, and organics have been detected in several samples of carbonates, sulphates and chloride minerals, which have allowed a distinction to be made between various evaporite classes mixed with the an algal mat. Overall, the multiple spectroscopic approaches presented have the potential for detection indicators of the forms of former life on Mars analogous to terrestrial extremophiles.

Acknowledgements

The author would like to thank Dr Bernard Hubbard from the United States Geological Survey, Reston, VA, and Dr Habes Ghrefat from the University of Texas at El Paso for their help in the spectral analyses of the samples presented in this study. Part of this work was financially supported by the Research Affairs at the UAE University under a contract no: 01-05-2-12/03.

References

Alsharhan, A.S. & Kendall, C.G.St C. (2002). Holocene carbonate/evaporites of Abu Dhabi, and their Jurassic ancient analogs. In *Sabkha Ecosystems*, eds Barth, H.J. & Boer, B., pp. 187–202. Kluwer Academic Publishers.

Arvidson, R.E., Poulet, F., Bibring, J.-P., Wolff, M.J., Gendrin, A., Morris, R.V., Freeman, J., Langevin, Y., Mangold, N. & Bellucci, G. (2005). Spectral reflectance and morphologic correlations in Eastern Terra Meridiani, Mars. *Science* **307**, 1591–1594.

Barancikova, G., Senesi, N. & Brunetti, G. (1997). Chemical and spectroscopic characterization of humic acids isolated from different Slovak soil types. *Geoderma* **78**, 251–266.

Bell, J.F. (1996). Iron, sulfate, carbonate and hydrated minerals on Mars. In *Mineral Spectroscopy: A Tribute to Roger G. Burns*, eds Dyar, M.D. *et al*., vol. 5, pp. 359–380. Geochemical Society, Al Ain, UAR.

Bibring, J.-P. *et al*. (2005). Mars surface diversity as revealed by the OMEGA/Mars Express observations. *Science* **307**, 1576–1581.

Bishop, J.L., Enver, M., Lan, M.D. & Mancinelli, F. (2004). Multiple techniques for minerals identification on Mars: a study of hydrothermal rocks as potential analogues for astrobiology sites on Mars. *Icarus* **169**, 311–323.

Christensen, P.R. (2003). Formation of recent martian gullies through melting of extensive water rich snow deposits. *Nature* **422**, 45–48.

Christensen, P.R. *et al*. (2004a). Initial results from the Mini-TES experiment in Gusev Crater from the Spirit Rover. *Science* **305**, 837–842.

Christensen, P.R. *et al*. (2004b). Mineralogy at Meridiani Planum from the Mini-TES experiment on the Opportunity Rover. *Science* **306**, 1733–1739.

Clark, B.C. (1993). Geochemical components in Martian soil. *Geochim.ica Cosmochim. Acta* **57**, 4575–4581.

Clark, B.C. & Van Hart, D.C. (1981). The salts of Mars. *Icarus* **45**, 370–378.

Clark, R.N. (1999). Spectroscopy of rocks and minerals and principles of spectroscopy. In *Remote Sensing for Earth Sciences: Manual of Remote Sensing*, 3rd edn, ed. Rences, A.N., vol. 3, pp. 3–52. John Wiley & Sons, New York.

Clark, R.N. & Roush, T.L. (1984). Reflectance spectroscopy: quantitative analysis techniques for remote sensing applications. *J. Geophys. Res.* **89**, 6329–6240.

Crowley, J.K. (1991). Visible and near-infrared (0.4–2.5 micron) reflectance spectra of playa evaporate minerals. *J. Geophys. Res.* **96**, 16 231–16 240.

Drake, N.A. (1995). Reflectance spectra of evaporite minerals (400–2500 nm): applications of remote sensing. *Int. J. Remote Sens.* **16**, 2555–2571.

Dreibus, G. & Wnke, H. (1990). Comparison of the chemistry of Moon and Mars. *Adv. Space Res.* **10**, 7–16.

Edwards, H.G.M., Moody, C.D., Newton, E.M., Villar, S.E.J. & Russel, M.J. (2005a). Raman spectroscopic analyses of cyanobacterial colonization of hydromagnesite, aputative Martian extremophile. *Icarus* **175**, 372–381.

Edwards, H.G.M., Villar, S.E.J., Jehlicka, J. & Munshi, T. (2005b). FT-Raman spectroscopic study of calcium-rich and magnesium rich carbonate minerals. *Spectrochemica Acta* A **61**, 2273–2280.

Evans, G. *et al*. (1969). Stratigraphy and geologic history of the sabkha, Abu Dhabi, Persian Gulf. *Sedimentology* **12**, 145–159.

Friedman, G.M. & Krumbein, W. (eds) (1985). *Hypersaline Ecosystems – The Gavish Sabkha; 484 S*. (*Ecological Studies*, vol. 53). Springer, Berlin.

Gaffey, S.J., McFadden, L.A., Nash, D. & Pieters, C.M. (1993). Ultraviolet, visible, and near-infrared reflectance spectroscopy: laboratory spectra of geologic materials. In *Remote Geochemical Analysis: Elemental*

and Mineralogical Composition, eds Pieters, C.M. & Englert, P.A.J., pp. 43–77. Cambridge University Press, Cambridge.

Gendrin, A. *et al.* (2005). Sulfates in martian layreed terrains: the OMEGA/Mars Express view. *Science* **307**, 1587–1591.

Gilmore, M.S., Merrill, M.D., Castino, R., Bornstien, B. & Greenwood, J.P. (2004). Effect of Mars analogy dust deposition on the automated detection of calcite in visible/near-infrared spectra. *Icarus* **172**, 641–646.

Hapke, B. (1993). Combined theory of reflectance and emittance spectroscopy. In *Remote Geochemical Analysis: Elemental and Mineralogical Composition*, eds Pieters, C.M. & Englert, P.A.J., pp. 31–42. Cambridge University Press, Cambridge.

Haskin, L.A., Wang, A., Rockow, K.M., Jolliff, B.L., Korotev, R.L. & Viskupic, K.M. (1997). Raman spectroscopy for mineral identification and quantification for in situ planetary surface analysis: a pointcount method. *J. Geophys. Res.* **102**, 19 293–19 306.

Howari, F.M., Goodell, P.C. & Miyamoto, S. (2003). Spectral properties of salt crusts formed on saline soils. *J. Environ. Qual.* **31**, 1453–1461.

Howari, F.M. (2004). Chemical and environmental implications of visible and near infrared spectral features of salt crusts. *J. Anal. Environ. Chem.* **94**, 315–323.

Hunt, G.R. (1982). Spectroscopic properties of rocks and minerals. In *Handbook of Physical Properties of Rocks*, ed. Carmichael, R.S., vol. 1, pp. 295–385. CRC Press, Boca Raton, FL.

Hunt, G.R. & Salisbury, J.W. (1970). Visible and near infrared spectra of minerals and rocks. I. Silicate minerals. *Mod. Geol.* **1**, 283–300.

Hunt, G.R., Salisbury, J.W. & Lenhoff, C.J. (1971a). Visible and near-infrared spectra of minerals and rocks. IV. Sulphides and sulphates. *Mod. Geol.* **3**, 1–4.

Hunt, G.R., Salisbury, J.W. & Lenhoff, C.J. (1971b). Visible and near-infrared spectra of minerals and rocks. III. Oxides and Hydroxides. *Mod. Geol.* **2**, 195–205.

King, P.L., Lescinsky, D.T. & Nesbitt, H.W. (2005). The composition and evolution of primordial solutions on Mars, with application to other planetary bodies. *Geochem. Cosmochim. Acta* **68(23)**, 4993–5008.

Klingelhöfer, G. *et al.* (2003). Athena MIMOS II Mössbauer spectrometer investigation. *J. Geophys. Res.* **108**, 8067.

Loh, E. (1973). Optical vibrations in sheet silicates. *J. Phys. C Solid State Phys.* **6**, 1091–1104.

Lane, M. & Christensen, P.R. (1998). Thermal infrared emission spectroscopy of salt minerals predicted for Mars. *Icarus* **135**, 528–536.

Landis, G.A. (2001). Martian water: are there extant halobacteria on Mars? *Astrobiology* **1(2)**, 161–164.

Mahaney, W.C., Milner, M.W., Netoff, D.I., Malloch, D., Dohm, J.M., Baker, V.R., Miyamoto, S., Hare, T.M. & Komatsue, G. (2004). Ancient wet Aeolian environment on Earth: clues to presence of fossil live microorganisms on Mars. *Icarus* **171**, 39–53.

McLennan, S.M. (2000). Chemical composition of Martian soil and rocks: complex mixing and sedimentary transport. *Geophys. Res. Lett.* **27**, 1335–1338.

McLennan, S.M. (2003). Sedimentary silica on Mars. *Geology* **31**, 315–318.

McSween, H.Y. Jr. (2002). The rocks of Mars, from far and near. *Meteor. Planet. Sci.* **37**, 7–25.

McSween, H.Y. Jr. & Keil, K. (2000). Mixing relationships in the Martian regolith and the composition of the globally homogeneous dust. *Geochim. Cosmochim. Acta* **64**, 2155–2166.

McSween, H.Y. Jr., Grove, T.L. & Wyatt, M.B. (2003). Constraints on the composition and petrogenesis of the Martian crust. *J. Geophys. Res.* **108**, 5135, doi: 10.1029/2003JE002175.

McSween, H.Y. Jr. *et al.* (1999). Chemical, multispectral, and textural constraints on the composition and origin of rocks at the Mars Pathfinder landing site. *J. Geophys. Res.* **104**, 8679–8715.

Metternicht, G. & Zink, A. (1997). Spatial discrimination of salt and sodium affected soil surfaces. *Int. J. Remote Sens.* **18**, 2471–2486.

Mougenot, B., Epema, G.F. & Pouget, M. (1993). Remote sensing of salt affected soils. *Remote Sens. Rev.* **7**, 241–259.

Mulders, M.A. (1987). *Remote sensing in soil science, developments in soil science*. Elsevier, Amsterdam.

Mustard, J.F., Poulet, F., Gendrin, A., Bibring, J.-P., Langevin, Y., Gondet, B., Mangold, N., Bellucci, G. & Altieri, F. (2005). Olivine and pyroxene diversity in the crust of Mars. *Science* **307**, 1594.

Pérez, M.G., Neto, L.M., Saab, S.C., Novotny, E.H., Débora, M., Miloria, B.P., Vanderlei, S.B., Luiz, A.C., Wanderley, J.M. & Heike, K. (2004). Characterization of humic acids from a Brazilian Oxisol under different tillage systems by EPR, 13C NMR, FTIR and fluorescence spectroscopy. *Geoderma* **118(3–4)**, 181–190.

Pierson, B.K. & Parenteau, M.N. (2000). Phototrophs in high iron microbial mats: microstructure of mats in iron-depositing hot springs. *FEMS Microbiol. Ecol.* **32**, 181–196.

Roush, T.L., Blaney, D.L. & Singer, R.B. (1993). The surface composition of Mars as inferred from spectroscopic observations. In *Remote Geochemical Analysis: Elemental and Mineralogical Composition*, eds Pieters, C.M. & Englert, P.A.J., pp. 367–393. Cambridge University Press, Cambridge.

Ruff, S.W. *et al.* (2001). Mars' "White Rock" feature lacks evidence of an aqueous origin: results from Mars Global Surveyor. *J. Geophys. Res.* **106**, 23 921–23 927.

Russell, N.C., Edwards, H.G.M. & Wynn-Williams, D.D. (1998). FT-Raman spectroscopic analysis of endolithic microbial communities from Beacon sandstone in Victoria Land, Antarctica. *Antarctic Sci.* **10**, 63–74.

Sadooni, F., Howari, F., Hamza, W. & Abd El-Gawad, E. (2005). Modern arid coastal sabkhas of the UAE: spatial and temporal evolution, sedimentology and geochemistry. In *The Sixth Annual U.A.E. University Research Conference, Research Affairs*, vol. 6, SC1–14, Al Ain, UAE.

Salisbury, J.W. (1993). Mid-infrared spectroscopy: laboratory data. In *Remote Geochemical Analysis: Elemental and Mineralogical Composition*, eds Pieters, C.M. & Englert, P.A.J., pp. 79–98. Cambridge University Press, Cambridge.

Sobalik, Z., Cejka, J. & Kribeack, B. (1998). Continuous monitoring of the oxidation of algal and humic-type kerogen in a heated FTIR flow cell. *Org. Geoch.* **28(11)**, 767–772.

Squyres, S.W. *et al.* (2004a). The Spirit rover's Athena science investigation at Gusev Crater, Mars. *Science* **305**, 794–799.

Squyres, S.W. *et al.* (2004b). The Opportunity rover's Athena science investigation at Meridiani Planum, Mars. *Science* **306**, 1698–1703.

Stevenson, F.J. (1994). *Humus Chemistry: Genesis, Composition, Reactions*. Wiley, New York.

Villar, S.E.J. & Edwards, H.G.M. (2005). Near-infrared Raman spectra of terrestrial minerals: relevance for remote sensing of Martian spectral signatures. *Vibrational Spectrosc.* **39**, 88–94.